International Journal of Crashworthiness

ISSN: (Print) (Online) Journal homepage: www.tandfonline.com/journals/tcrs20

Investigate the elastoplastic deformation behaviour of a motorcycle frame under different mechanical load configurations

Markus Fasching, Alessio Severin & Christian Ellersdorfer

To cite this article: Markus Fasching, Alessio Severin & Christian Ellersdorfer (2024) Investigate the elastoplastic deformation behaviour of a motorcycle frame under different mechanical load configurations, International Journal of Crashworthiness, 29:2, 308-319, DOI: 10.1080/13588265.2023.2241224

To link to this article: https://doi.org/10.1080/13588265.2023.2241224

Published online: 09 Aug 2023.

INTERNATIONAL JOURNAL OF CRASHWORTHINESS
2024, VOL. 29, NO. 2, 308–319
https://doi.org/10.1080/13588265.2023.2241224

Investigate the elastoplastic deformation behaviour of a motorcycle frame under different mechanical load configurations

Markus Fasching, Alessio Severin and Christian Ellersdorfer

VSI - Vehicle Safety Institute, University of Technology Graz, Austria

ABSTRACT

This study investigates the elastoplastic deformation behaviour of a motorcycle frame under quasi-static mechanical loading. We present a novel test rig to analyse the mechanical integrity of a motorcycle frame under four different load configurations. These four load configurations reproduce longitudinal forces, lateral forces, torques and bending moments that act on the frame in normal operation as braking, acceleration or cornering. Additionally, the four load configurations represent loads that act on the frame in the most frequent crash scenarios in urban areas, such as a motorcycle's frontal or inclined collision against a car. We conducted three repetitions of each load configuration with a frame from a motorcycle, especially for the urban area. The compliance of the measured load–displacement curves is rated by an objective assessment method. All tested frames show a similar elastoplastic deformation pattern; specifically, the longitudinal tubes are pressed outside, and fractures occur predominantly at areas of welding spots while the inner part remains scarcely deformed. The load–displacement curves, mechanical failures, weak points and deformation behaviour of the frames can be used in future to validate a numerical model of a motorcycle frame and improve the crashworthiness of a motorcycle frame.

HIGHLIGHTS

- Novel experiments on the elastoplastic characterisation of motorcycle frames
- Multidirection deformation and failure behaviour
- Motorcycle frame as protection for sensitive components such as batteries
- Approach to validate deformation patterns and mechanical resistance of simulation models
- Validation of the test reproducibility by compliance assessment of measurement data

ARTICLE HISTORY
Received 1 June 2022
Accepted 20 July 2023

KEYWORDS
Powered-two-wheeler; motorcycle; crashworthiness; frame; experimental investigation; quasi-static

1. Introduction

The stiffness of a motorcycle frame strongly influences the vehicle's driving behaviour [1]. The flexional and torsional stiffness of the motorcycle frame affect the wobble frequency and damping and can improve the motorcycle's stability [2,3]. The frame is also one of the main safety components in durability terms due to its absorption of loads that the motorcycle is exposed to during its lifetime [4]. For this reason and also because of product liability [5], the elastic response of motorcycle frames is widely analysed to assess the dynamic response of the vehicle. Furthermore, the fatigue life of the frame is studied to guarantee a faultless function over the lifetime of a motorcycle [6]. In the event of a crash, high mechanical loads act on the motorcycle frame and can lead to plastic deformations of the frame [7]. These deformations can penetrate inner placed components of the frame, for example, a traction battery in the case of an electric-powered motorcycle. The penetration of a traction battery can lead to an external or internal short circuit of the battery cells in the traction battery, and the separator can get damaged [8–14]. Subsequently, a damaged separator triggers an uncontrolled exothermic reaction (Thermal Runaway [15,16]) that results in fire or explosion of the traction battery [9,11,12,17]. The released gases are extremely dangerous and harmful to humans and the environment [18]. To Increase the crashworthiness of a motorcycle, the frame can be seen as a structure to absorb deformations and loads [9]. Therefore, the motorcycle frame is a relevant component that influences the stability and crashworthiness of the motorcycle.

1.1. Mechanical normal operating loads

Loads generated by normal usage (e.g. acceleration, cornering or braking) or in non-ordinary driving manoeuvres [19] (e.g. passing kerbs, maximum acceleration or straight-line braking) are referred to as normal operating loads. Fatigue tests investigate the influence of normal operating loads in the form of high-cycle loads with representative load collectives [20]. These load collectives are derived from the loads occurring in field tests through the obtained mileage, as Petrone et al. [4,5] mainly reported for the European market.

CONTACT Markus Fasching fasching@tugraz.at; Christian Ellersdorfer christian.ellersdorfer@tugraz.at

The maximum expectable force acting on the motorcycle frame in the longitudinal direction in normal usage or non-ordinary driving scenarios is approximately 40 kN in the case of passing a deep pothole [5]. The maximum expectable vertical force is around 2.8 kN when driving over a kerb [19]. In addition to the longitudinal and vertical forces reported in the open literature, lateral forces can also act on the motorcycle frame (e.g. cornering). However, the open literature does not propose information about the occurring forces that act on the frame laterally during normal operation. Nevertheless, the lateral tyre characteristics are well described in different literature. For instance, Cossalter et al. [21], de Vries and Pacejka [22] and Pacejka [23] report lateral forces up to 4.1 kN acting on the tyre during cornering. The lateral tyre forces create forces and moments on the steering head. Thus, under the consideration of the equilibrium of the motorcycle in a curve and the motorcycle geometry (wheelbase, trail, etc.), the acting forces on the motorcycle frame can be determined. [2] Additionally, the motorcycle frame can be loaded by a torque of 1.0 kNm [19] in motorcycle competition and a bending moment of approximately 1.8 kNm when driving off-road [4]. For a torque around the vertical axis, no values could be found in the literature.

Bocciolone et al. [24] and Cossalter [2] describe a test setup suitable for analysing static together with dynamic properties of the plain frame and the frame with the installed engine under loads occurring during normal operation. Moreover, specific test setups have already been proposed for investigating the fatigue strength of almost the entire motorcycle (assembly of steering fork, frame, swing arm, rear wheel, rear body and seat structure) either with [5] or without the engine [4]. Other studies confirm the importance of understanding the deformation behaviour also of other motorcycle components. For example, Cossalter et al. [25] characterise the static and dynamic deformability of the front fork under lateral loading, and Tan et al. [26] investigate the deformation behaviour of front wheel-tyre assembly when it is subjected to frontal impact loading.

The open literature proposes forces and moments acting on the motorcycle frame and their influence on the fatigue life, and the mechanical properties of different motorcycle frames is investigated with suitable test rigs.

Virtual simulations are just as important as experimental testing in vehicle development in today's world. For the creation of realistic and precise simulation models the studies of Ballo et al. [19], Bocciolone et al. [24] and Cossalter et al. [25] pointed out the need for experimental investigations to validate and prove a realistic deformation behaviour of the virtual models. In virtual models, the influence of different parameters (e.g. cross section or wall thickness of a tubular frame) on the mechanical behaviour like stiffness can easily be estimated [6,27]. For normal operating loads, the literature, e.g. [4,5,19,20,24] proposes testing methods and test rigs to investigate the mechanical behaviour.

1.2. Crash loads

The majority of motorcycle accidents (50% [9] – 72.3% [28]) occur in urban areas, where cars are the most frequent collision partner, accounting for 44.2% to 70% [9,28,29]. For crash scenarios with a car as an opponent vehicle, the frontal collision of a motorcycle against a car's side (45%), the frontal collision of a motorcycle against a car's front (20%) and the frontal collision of a motorcycle against a car's rear (10%) represent 75% of all crash scenarios in the urban area [30]. Therefore, the first collision contact results in the motorcycle's front wheel with a load introduction in the longitudinal direction of the motorcycle [9,28,30–32]. If the motorcycle collides with a car not in a straight-line but at an angle, then, a lateral force or torque can act on the frame. Additionally, a lateral force or torque can act on the frame when a car hits the motorcycle's side (7.5% in an urban area [30]) in the front area. For motorcycle accidents with an opponent vehicle, 78% of all accidents have an impact velocity below 50 km/h [28]. Therefore, the urban area's relevant impact velocities are 36 km/h [9] and 48 km/h [32]. Compared to normal operating loads, crash loads are generally higher. They can lead to plastic deformation that results in a failure of the frame (see top two pictures in Figure 1) and the whole motorcycle (e.g. wheels, fork, etc.) [7,33]. However, while statistically frequent crash scenarios [28,30] and the corresponding impact velocities for urban areas can be found in the literature [32], the literature does not propose the loads that act on the motorcycle frame in terms of magnitude, direction (e.g. lateral or longitudinal) or configuration (force or moment) in the event of a crash.

Tests with full vehicles are performed to investigate the mechanical behaviour and crashworthiness of a motorcycle and its components based on crash loads [7]. Ellersdorfer et al. [10] conducted full vehicle crash tests with an electric motorcycle to find weaknesses in the traction battery. For this purpose, 3D scanning techniques are used to find deformations of the traction battery after the crash tests. However, no external plastic deformations of the traction battery pack housing were detected when the frame became deformed (see Figure 1) [34]. This confirms the suitability of the frame as a protective structure. Under this point of view, Sevarin et al. [35] and Fasching [36] propose integrating a battery pack in electric-powered motorcycles as a structural component by merging the battery pack housing and the motorcycle frame.

Figure 1 compares an experimental test and a virtual simulation for the most frequent crash scenario of a motorcycle. Longitudinal forces, respectively, a bending moment that is introduced on the frame over the steering head, lead to high plastic deformation in the front area of the frame. The tubes at the steering head buckle under the longitudinal load and bulge. From Figure 1, it is also evident that the largest deformation occurs in the front part of the frame and at the side tubes. No deformation can be obtained visually at the rear frame. The simulation model is validated by comparing the deformations and the measured parameters (e.g. accelerations) from experimental tests to those of the simulation [9,37]. With simulations, the deformation history, the material failure and the absorbed energy of the frame can be analysed in detail for different crash scenarios.

Figure 1. Most frequent motorcycle crash scenario (frontal collision of a motorcycle against a car): comparison of the test (top two pictures) and simulation (bottom two pictures) [37].

Thus, simulations show if occurring deformations of the frame penetrate inner placed components (e.g. a traction battery as Figure 1 shows) and the crashworthiness can be analysed and assessed. [27,38]. Virtual simulation can also be used, to investigate the influence of energy-absorbing structures or geometrical changes in the frame (e.g. cross section) on the crashworthiness [6,39]. Therefore, the simulations are used to assess the crashworthiness and improve it. However, the studies only mention full vehicle tests but none mention or investigate the elastoplastic deformation behaviour of the frame as an isolated component under mechanical loads that can occur during a crash.

Realistic and precise simulation models are necessary to evaluate the crashworthiness of conventional motorcycles as well as electric-powered motorcycles. For this, it needs dedicated test rigs to investigate the frame's behaviour inaccurate experimental tests. Tests of the isolated frame under high mechanical loads with precise and reproducible boundary conditions are the basis to verify and validate the simulation model according to deformation patterns and measurement data. [6]

Existing test rigs and procedures investigate the fatigue behaviour of a motorcycle with representative load collectives of normal operating loads. However, the influence of higher loads that occur in crash scenarios is only investigated in full vehicle crash tests, but the frame as an isolated component is not investigated in the open literature. Therefore, no appropriate test rig and associated measurement system exist to cause elastoplastic deformations on a motorcycle frame as an isolated component under quasi-static mechanical loading. To fill this research gap, in this study we:

- Investigate the first time the deformation behaviour of a motorcycle frame as an isolated component.
- Present a self-developed novel test rig and apply loads on the frame with magnitudes multiple times larger than those occurring in normal operations.
- Investigate the elastoplastic deformation behaviour of a motorcycle frame to cover the elastic and plastic deformation range within one experiment.
- Conduct, as the first, four different load configurations which represent loads occurring in normal operation as well as in the most frequent crash scenarios for on-road urban areas.
- Propose a new measurement method for the developed test rig to measure the frame-only deformations without the influence of the elastic deformation of the test rig.
- Provide high-quality measurement data and the deformation patterns of the elastoplastic behaviour of the frame to develop and validate a crash simulation model of a motorcycle frame in future.

- Show information about the weak points of the frame due to the elastoplastic deformation range that can be used to improve the crashworthiness (e.g. changing the geometry or additional stiffeners).

2. Method

The considered specimen is the frame of the Husqvarna Vitpilen 401. The Husqvarna Vitpilen 401 has a power of 32 kW and an engine displacement of 373 cm^3. Therefore, it represents a medium-power on-road naked bike and is suitable especially for an urban area. The plain frame itself has a complex welded multitube trellis structure and is made of 25CrMo4 steel. The frame's geometry defines the attachment points to the swing arm and the steering head. We investigate the elastoplastic mechanical behaviour of the frame in four different load configurations with three repetitions each.

2.1. Mechanical load configurations

To investigate the elastoplastic deformation behaviour of the frame, the load configurations are chosen to represent loads acting on a frame in everyday usage and crash scenarios of urban areas. Because the loads on the frame are introduced over the steering head for normal operating loads and crash loads, they differ in magnitude, but they can be summarised in a simplified way in the same load configurations. As aforementioned, longitudinal forces, lateral forces, torques and bending moments can act on the motorcycle frame in normal operation and crash scenarios. Therefore, the four load configurations (depicted in Figure 2) are defined as follows:

- ***V1*:** A longitudinal force represents normal operation loads in the longitudinal direction of the motorcycle, such as accelerating, braking or passing potholes. It also represents the force introduced over the steering head in a straight-line collision of a motorcycle against a car. The specimens are named Frame 1–3.
- ***V2*:** A lateral force represents normal operation loads in the lateral direction of the motorcycle, such as cornering. In the case of cornering, the force is transmitted from the tyre over the fork to the steering head. Additionally, lateral forces can act on the steering head in a simplified way when a car collides with the front area of the motorcycle (e.g. front wheel, fork) or in an inclined collision of a motorcycle against a car. The specimens are named Frame 4–6.
- ***V3*:** A torque represents normal operation loads in case of cornering and, in a simplified way, also crash loads (car collides to the front area of the motorcycle and inclined collision of a motorcycle against a car). The lateral forces acting on the tyre or front wheel are transmitted over the fork to the steering head, resulting in torque due to the lever arm. The specimens are named Frame 7–9.
- ***V4*:** A bending moment represents normal operation loads such as accelerating, braking or passing potholes and the force of a straight-line collision. The longitudinal forces acting on the front wheel introduce a bending moment on the steering head. The specimens are named Frame 10–12.

2.2. Test setup

To investigate a motorcycle frame's lateral, longitudinal and torsional stiffness, Cossalter [2] proposes to lock the swing arm pivot and introduce the loads over the steering head. Existing studies investigate only the torsional (*V3*) and flexural stiffness (*V4*) for a frame as an isolated component [24]. Other studies [4,5] propose a test setup to investigate the longitudinal force in combination with the bending moment for normal operating loads. However, in the open literature, no study that investigates all four load

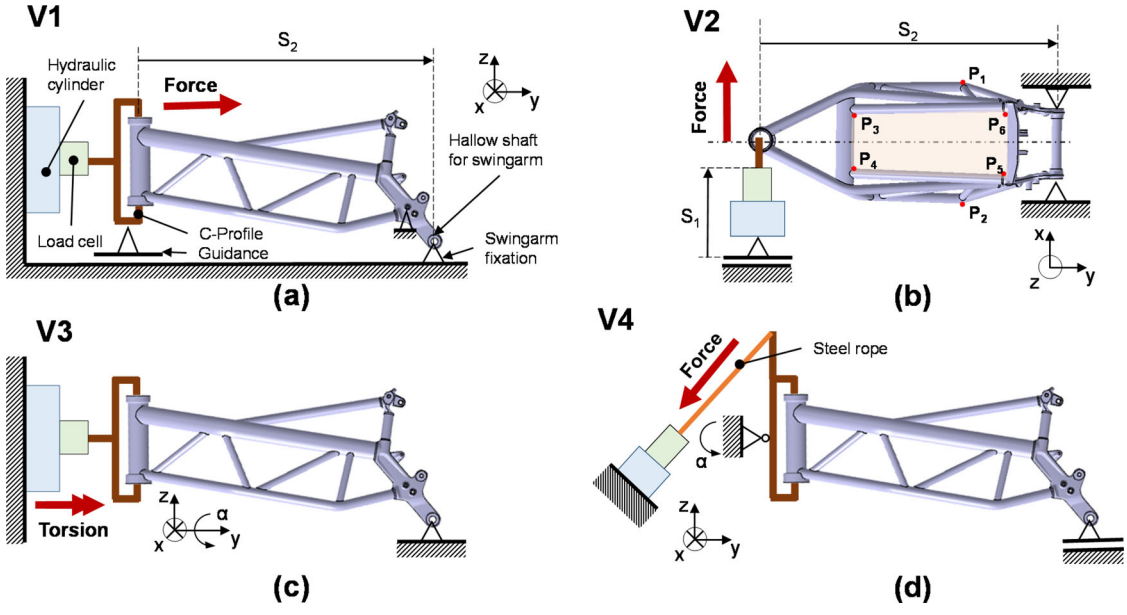

Figure 2. Schematic sketch of the force introduction, the fixation and the measured displacements of the frame for the four load configurations: (a) *V1* (longitudinal force), (b) *V2* (lateral force), (c) *V3* (torque) and (d) *V4* (bending moment).

configurations for a motorcycle frame or proposes an appropriate test rig can be found. Therefore, we developed a dedicated test rig to investigate the elastoplastic deformation behaviour of a motorcycle frame in the four defined load configurations under quasi-static loading conditions. In the construction (dimensions and material selection) of the test rig, it was proven that none of its parts was plastically deformed during loading. Quasi-static tests neglect the strain rate influences. However, they can still be used as input for virtual crash simulation because the strain rate dependency is a material parameter that can be evaluated separately.

2.2.1. Load introduction

Similar to previous studies [2,4,5,24], we introduce the load over the frame's steering head with a manually operated hydraulic cylinder Yale YH-20/250 (Columbus McKinnon Industrial Products GmbH). Therefore, the hydraulic cylinder is connected to the C-Profile that applies the load on the steering head. The C-Profile is guided in different ways to ensure the application of a pure translational force, respectively, moment depending on the load configuration:

- ***V*1:** To ensure a pure translational force introduction in the longitudinal direction (y-axis), the C-Profile is guided by profiled rail guides (named as guidance in Figure 2(a)) with only one degree of freedom in the longitudinal direction.
- ***V*2:** To ensure a pure translational force introduction in the lateral direction (x-axis), the C-Profile is guided by two 90° offset rail guides. In this configuration, the frame's steering head can move freely in the longitudinal and lateral directions.
- ***V*3:** To ensure a pure torque on the steering head, a shaft guided by ball bearings introduces a rotation of the C-profile around the y-axis (Figure 2(c)).
- ***V*4:** To ensure a pure bending on the steering head, also a shaft guided by ball bearings introduces a rotation of the C-profile, but around the x-axis (Figure 2(d)).

2.2.2. Fixation of frame

The fixation, as shown in Figure 2, is defined by the frame geometry at the hollow shaft where the swing arm of the motorcycle is connected to the frame. A rotational movement of the frame is allowed by pivoted fixation. Only for $V1$, the frame is additionally clamped to lock a rotation comparable to Cossalter [2].

The swing arm fixations block any translational movement for $V1$, $V2$ and $V4$ according to the loading condition 'locked swing arm pivot', described by Cossalter [2]. For $V4$, the swing arm fixations are guided by rail guides to allow only a movement in the y-axis of the frame. Allowing a translational movement ensures that the steering head can rotate freely [24] in $V4$.

2.2.3. Measurement system

The applied load is measured with a load cell type HBM C6A 500 kN (accuracy 0.05%; Hottinger Brüel & Kjaer GmbH) for load configurations $V1$ and $V2$. For the load configurations $V3$ and $V4$, the load cell type GTM Serie K 63 kN (accuracy 0.03%; GTM Testing and Metrology GmbH) is used.

The test rig will deform elastically during the test due to the applied loads. To overcome the influence of the elastic test rig deformation on the force–displacement curve of the frame, we use a dedicated measurement method (Figure 2). This measurement method allows us to measure the frame-only deformation without the influence of the elastic test rig deformation. The usage of two String Potentiometer 'S_1' (ASM WS10-1250-R1K-L10-M4-D8-HG; accuracy 0.04%; ASM GmbH) and 'S_2' (ASM WS10-500-R1K-L10-M4-M12-HG; accuracy 0.08%; ASM GmbH), as well as an angle sensor Gefran PR-65-E-0-103 (accuracy 0.018%; GEFRAN spa) allow an accurate displacement measurement. The measured data is monitored with the data acquisition system DEWE − 2600 in combination with DAQP-STG modules (both Dewetron) with a measurement frequency of 1 kHz.

Figure 2 shows the translational displacements S_1 and S_2 for $V1$ and $V2$, as well as the rotation angle α for $V3$ and $V4$. The declaration of the metrics is named regarding the measurement devices S_1, S_2, respectively, α (angle sensor).

2.3. Pre-and post-measurements

Figure 2(b) shows a schematic sketch of the considered frame with the measurement points P_1 to P_6 that are compared before and after the tests to obtain the plastic deformations. The distance $\overline{P_1P_2}$ is the maximum frame width, and $\overline{P_3P_4}$, $\overline{P_4P_5}$, $\overline{P_5P_6}$, $\overline{P_6P_3}$ define a trapezium that can be seen in orange in Figure 2(b). The distances of the un-deformed frame are $\overline{P_1P_2} = 259$ mm, $\overline{P_3P_4} = 115$ mm and $\overline{P_5P_6} = 134$ mm with a tolerance of ± 3 mm according to the manufacturing drawing. The distance $\overline{P_3P_6} = \overline{P_4P_5} = 320$ mm has a tolerance of ± 0.506 mm.

The distances of the un-deformed frame before the experiment and the deformed frame after the experiment are compared. The relative change is calculated to quantify the occurring deformations.

2.4. Test procedure

2.4.1. Pre-loading

In the test setup, a clearance can exist due to the manufacturing tolerances of the frame and the test rig components. We execute a pre-loading before each experiment to eliminate the clearance and its influence on the test results. The range of the possible clearances was determined based on the manufacturing tolerances of the frame and the test rig components for each test configuration:

- $V1$: 0.231–2.061 mm
- $V2$: 0.231–1.161 mm

- $V3$: 0–0.442°
- $V4$: 0–0.554°

The different clearance ranges arise because different components are used in the four load configurations. In pre-loading, a force termination criterion of 5% of the expected yield load prevents damage to the specimen due to excessively high loads in case of a smaller clearance [32]. Since the maximum expected load on the frame is unknown, and the literature suggests no reference values, we defined the force termination criterion as 10% of the maximum load occurring in normal operation. We use for $V1$ the longitudinal force of 40 kN, for $V3$ the torque of 1 kNm and for $V4$ the bending moment of 1.8 kNm as reference for the termination criterion. No values are proposed in the open literature for the lateral forces acting on the frame during normal operation. Therefore, we take the lateral tyre force of 4.1 kN during cornering as the reference value in $V2$. We made this simplifying assumption in the lateral direction because we need a reference value to calculate the pre-load thresholds. The authors assume that this simplification does not influence the elastoplastic deformation behaviour because the displacement threshold also limits the pre-loading to prevent damage to the frame.

The combination of the maximum clearance and the force termination criterion defines the displacement and force thresholds in pre-loading, listed in Table 1. The defined thresholds ensure that the deformation of the frame remains in the elastic range, in any case, during pre-loading.

2.4.2. Loading thresholds

The motorcycle frame is loaded until the maximum load or displacement is reached to investigate the elastoplastic deformation behaviour. A hydraulic cylinder with a maximum force of 200 kN applies the loads on the motorcycle frame. Therefore, the test rig was designed and dimensioned to withstand the loading configurations without any plastic deformation based on the maximum applicable force by the hydraulic cylinder. Therefore, the force in the longitudinal ($V1$) and lateral ($V2$) load configuration is limited to 200 kN. For configurations $V3$ and $V4$, the chosen 63 kN load cell limits the maximum applicable load to 23.5 kNm. The maximum applicable torque is for $V3$ still approximately 23 times, and the bending moment for $V4$ is 13 times higher than the maximum load expected in normal operation.

The test rig's geometry limits the maximum applicable displacement to 78 mm in case of translational displacement in $V1$ and $V2$. The rotational displacement is limited to a maximum rotation angle of 26° for the load configurations $V3$ and $V4$, also pre-defined by the test rig's geometry.

Table 1. Thresholds for the displacement and force in pre-loading.

	$V1$	$V2$	$V3$	$V4$
Force threshold	4.000 kN	0.410 kN	0.100 kNm	0.180 kNm
Displacement threshold	2.061 mm	1.161 mm	0.442°	0.554°

Table 2. Expected maximum force in normal operation for all four conducted test configurations and the considered limits in the conducted experiments.

	$V1$		$V2$		$V3$		$V4$	
Load in normal operation	40 kN	[5]	4.1 kN	*	1.0 kN	[19]	1.8 kN	[4]
Force threshold	200 kN					23.5 kNm		
Displacement threshold	78 mm					26°		

*For $V2$, an assumption was made based on lateral tyre forces because no values could be found in the literature for this scenario.

Table 2 lists the maximum forces acting on the frame in normal operation and the loading thresholds within the experiments.

2.5. Compliance assessment of the load–displacement measurement

The CORAplus tool [40] compares and assesses the reproducibility of the measured load–displacement curves. CORrelation and Analysis (CORA) method [41] is an objective comparison method to assess the quality of compliance of two non-ambiguous signals (e.g. force–displacement curves) [41,42]. The CORA method consists of four independent procedures in which the agreement for the curves' size, phase, shape and corridor is evaluated separately [41]. An overall score R according to ISO/TR-9790 is calculated by a weighted average and divided into five categories [41,43,44]:

1. Excellent $0.86 \leq R \leq 1.00$
2. Good $0.65 \leq R < 0.86$
3. Fair $0.44 \leq R < 0.65$
4. Marginal $0.26 \leq R < 0.44$
5. Unacceptable $0.00 \leq R < 0.26$

The manual of the CORAplus tool [45] recommends values for the parameters. These parameters are applied in the open literature [44,46]. The CORA method is also implemented in different norms such as ISO/TR-9790 or ISO/TS 18571:2014 [47] or applied in different studies [43]. In the norms and studies, small adoptions of the parameter values are made. We evaluated the experiments in this study with the CORAplus tool with the proposed values from the manual and with the values from the norms. Therefore, we identified that the different parameter values result only in negligible influence (<2%) on the total score. For this reason, we used the parameters from the manual [45], with one exception for b_0. We chose a smaller value, b_0, to reduce the outer corridor to 0.3 instead of 0.5. The used values are listed in Table 3.

Table 3. CORA – Parameters based on the user's manual [45].

Parameter	Value	Parameter	Value	Parameter	Value	Parameter	Value
Y Norm	extremum	a_0	0.05	b_0	0.30	G1	0.50
G 2	0.50	d_min	0.01	d_max	0.12	G_V	0.50
G_G	0.25	G_P	0.25	K	2.00	K_V	10.0
K_G	1.00	K_P	1.00	INT_MIN	0.80	WF_Norm	YES
MIN_Norm	0.00						

3. Results

The force applied by the manually operated hydraulic cylinder results in a pulsating force progression. The maximum deviation force caused by this pulsating is at a maximum of 3% of the applied force. Thus, the force signals were smoothed using the software 'Diadem 2020' (National Instruments).

3.1. Pre-loading

The pre-loading is terminated by the force termination criterion for all experiments because the force threshold is exceeded before the displacement threshold is reached. For this reason, we applied the in Table 4 listed force and displacement offsets for the experiments. For all load configurations, the displacement values in pre-loading are well in the possible range of the calculated clearance.

3.2. Load–displacement curves

From Figure 3, it is apparent that for all four load configurations, the progression of the load–displacement curve can be divided into a linear part and a nonlinear part. The change in progression from a linear to a nonlinear slope occurs at an approximate load of 60 kN for *V*1, 4 kN for *V*2, 1.5 kNm for *V*3 and 8 kNm for *V*4.

In *V*1, the force–displacement curves of the three tests have a maximum force difference of only 2% up to a displacement of 4.2 mm. Until the maximum expectable longitudinal load in the normal operation of 40 kN, all curves show a similar and linear progression. An abrupt drop in force occurs for all three tests at a similar maximum force of about 90 kN. This drop results from a mechanical failure of the bearings, which lock the rotation of the frame around the hollow shaft (see Figure 2(a)) on both sides. For Frame 1 and Frame 3, both bearings (on the left and right frame side) break simultaneously, whereas for Frame 2, one bearing breaks at 18.4 mm, and the second bearing breaks at 30.3 mm. After this drop in force, it is visible that the side tubes are already pressed out, while the force stays almost constant.

In *V*2, the force–displacement curves of all tests have the same progression over the entire displacement with a shifted magnitude of force. No mechanical failure of any bearing or frame occurs during the entire test. The maximum force at a lateral displacement of 78 mm shows a difference of 1 kN between Frame 5 and Frame 6.

In *V*3, Frame 7 and Frame 8 have the same progression but, similar to *V*2, are shifted in terms of magnitude. It is

Table 4. Offsets of all tests.

	*V*1			*V*2			*V*3			*V*4		
Frame	1	2	3	4	5	6	7	8	9	10	11	12
Force offset (kN) or (kNm)		4.00			0.41			0.10			0.18	
Displacement offset (mm) or (°)	0.73	0.74	0.54	0.52	0.56	0.37	0.03	0.02	0.03	0.42	0.37	0.33

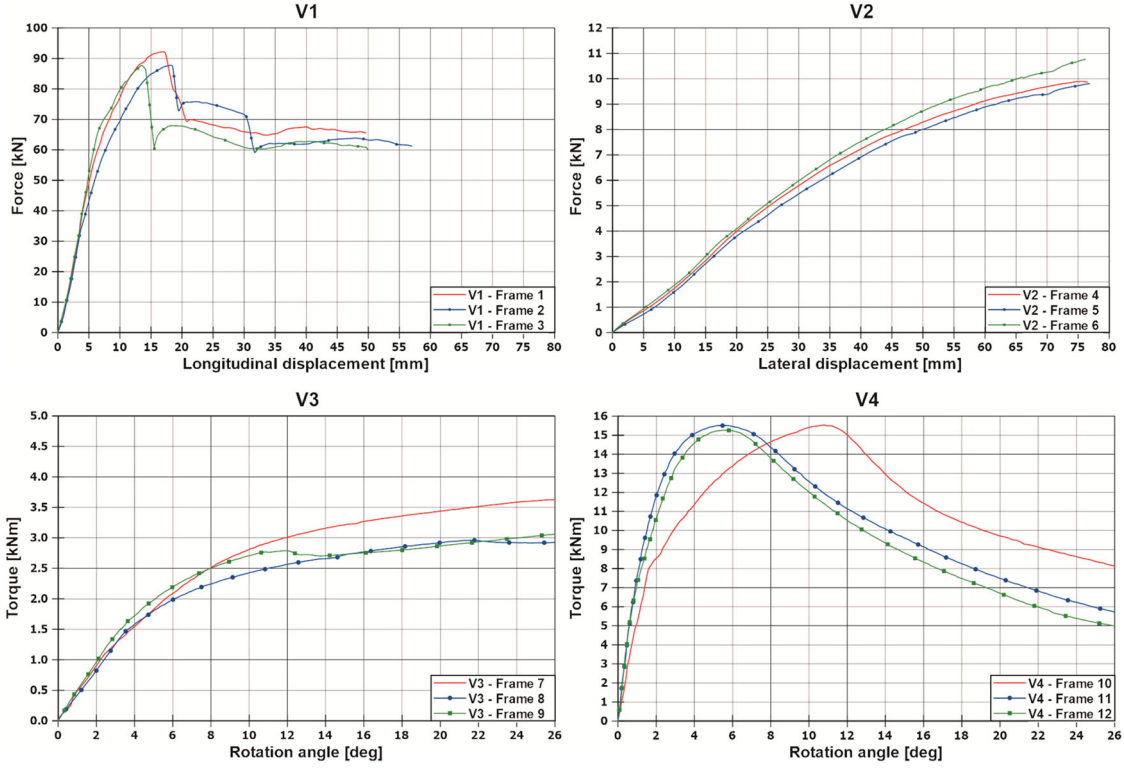

Figure 3. Force–displacement curve of *V*1 and *V*2 and torque–rotation angle curve of *V*3 and *V*4.

observable that Frame 9 shows a different behaviour than the others, with a force drop at 12° before a further rise of torque. The maximum torque at a rotation angle of 26° spreads 0.7 kNm between Frame 7 and Frame 8.

In *V*4, Frame 11 and Frame 12 have the same behaviour in the linear part, whereas Frame 10 has a slightly flatter slope in the linear progression up to 8 kN. After 8 kN, it is noticeable that Frame 11 and Frame 12 have a similar progression while Frame 10 behaves differently. The maximum torque of all three tests is comparable, but it is shifted by 6° for Frame 10.

3.3. Deformation behaviour of frame

Figure 4(a) shows a motorcycle frame in *V*1 in an un-deformed state before the test compared to the deformed state in Figure 4(b) after the test. Generally, within a load configuration, all three tests show the same deformation pattern. It is also noticeable that the inner part of the frame (orange-coloured trapezium in Figure 2(b)) is optically hardly deformed for all performed tests, supported by post-measurements. The distances of $\overline{P_3P_4}$, $\overline{P_5P_6}$, $\overline{P_3P_6}$ and $\overline{P_4P_5}$ change at a maximum of 2% for *V*1, 1% for *V*2, 2.7% for *V*3 and 4.3% for *V*4. The distance $\overline{P_1P_2}$, conversely, behaves differently for the different load configurations because of the different deformation behaviours of the frame.

In *V*1, the frames deform on the sides where the tubes are pressed outside and in the swing arm pivot area. At around 5 mm displacement, the side tubes begin to deform visually (red arrows in Figure 4(b)), and after 8 mm, the first fractures become visible (green cycles in Figure 4(b)). The fractures occur in the connection areas between the tubes of the tubular trellis steel frame. It is noticeable that the fractures do not occur directly at the welding spots, as Figure 4(f) shows exemplarily for Frame 1 in *V*1. The distance $\overline{P_1P_2}$ (Figure 2(b)) increases by up to 54% for all three tests caused by the pressed outside tubes.

In *V*2, the largest deformations occur in the area where the swing arm is attached (red arrows in Figure 4(c)). Due to the moment acting on the shaft at the fixation, the shaft gets deformed and moves counterclockwise at the area marked with red arrows in Figure 4(c), which becomes visible at a lateral displacement of 20–25 mm. The geometry of the deformed shaft is given by the frame geometry. The shape of the other frame parts scarcely shows deformations in their entirety, where the distance $\overline{P_1P_2}$ changes just around 2.5% for all three tests. After the tests, no fractures were visible on the frames.

In *V*3, the largest deformations also occur in the area where the swing arm is attached (red arrows in Figure 4(d)). The shaft gets deformed and rotates minimally counterclockwise. It is also evident that the rear shaft at the swing arm connection was plastically deformed. Nevertheless, the remaining frame stays almost completely un-deformed with a maximum change of distance $\overline{P_1P_2}$ of around 1.9% in all three tests. For Frame 7 and Frame 8, small fractures occur (green cycle in Figure 4(d)), whereas for Frame 9 the fracture separates almost the entire tube except for a 5–7 mm millimetres.

In *V*4, the frames deform in the first third of the frame (near the steering head), where the tubes and the sheet between them buckle (see red arrow and top green circle in Figure 4(e)). The side tubes are pressed outside, similar to the deformation pattern in *V*1. Again, the inner part of the

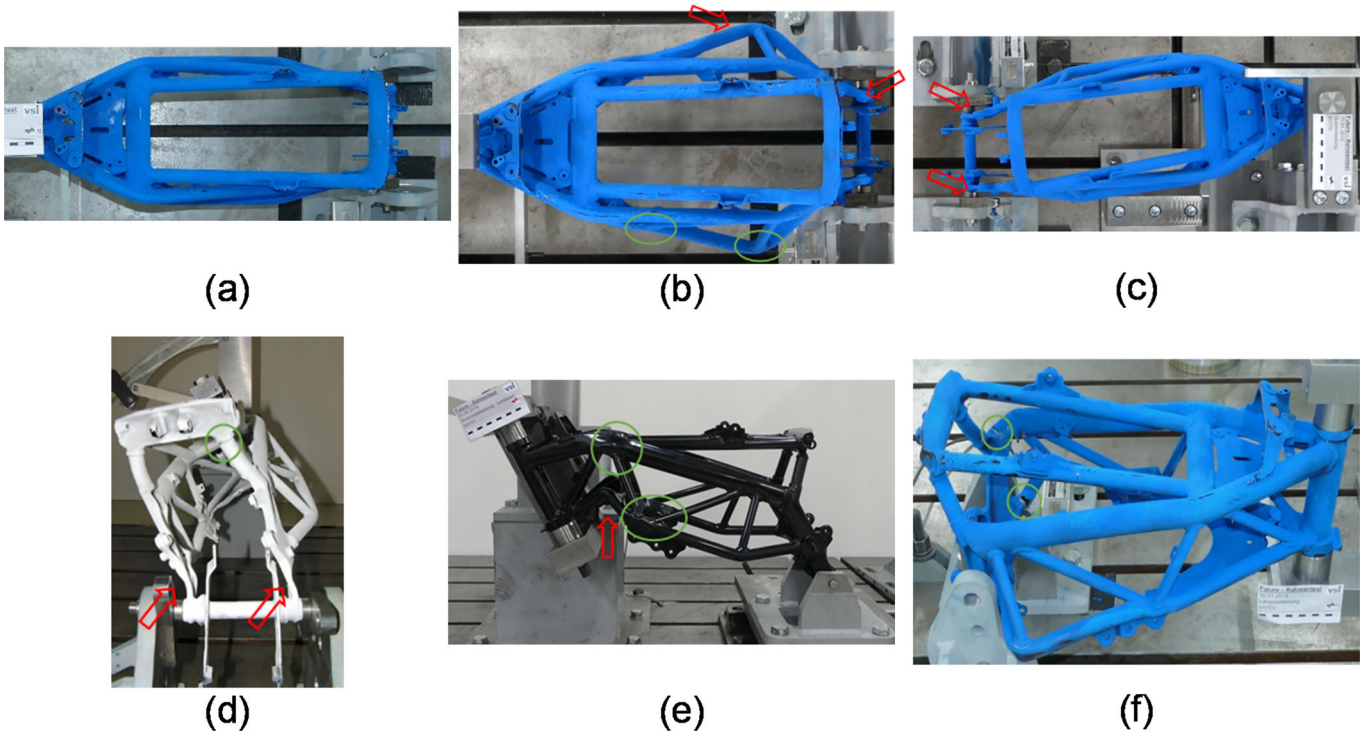

Figure 4. Exemplary photographs from the tests: (a) Un-deformed frame of *V*1 (b) deformed frame of *V*1 (c) deformed frame of *V*2 (d) deformed frame of *V*3 (e) deformed frame of *V*4 (f) typical areas of fractures.

frame stays nearly un-deformed while the distance $\overline{P_1P_2}$ increases by up to 18.9% for all three tests. Also, fractures occur at the connection areas between the tubes, marked by green cycles in Figure 4(e). Although the load–displacement curve for Frame 10 differs from Frame 11 and Frame 12, the deformation pattern is similar for all three frames.

3.4. Compliance assessment of test curves

Table 5 shows the results of the CORrelation and Analysis (CORA) method processed with the CORAplus tool [40] using the parameter stated in Table 3. The first test of each configuration was compared with the remaining two curves as reference data. The results underlie the optical impression that the tests have good reproducibility. Especially the repetitions of *V*2 and *V*3 have an excellent rating according to the score proposed by Gehre et al. [41]. The tests of *V*1 have similar progressions, but the maximum force differs between the repetitions and the displacement at maximum force. Therefore, *V*1 has good compliance. For the repetitions of *V*4, the size, phase and shape individually have an excellent rating. Still, as shown in Figure 3, the curve of Frame 10 has a different progression, resulting in a fair rating for the corridor method. The total rating of all load configurations results in a score of 0.855, which means good compliance, but it has to be noted that an excellent score is declared as a value of 0.86.

3.5. Limitations

The investigated motorcycle frame is from a medium-powered naked bike, especially for urban areas. Therefore, only urban on-road operation and crash scenarios for the urban area are analysed. Load scenarios in off-road driving or off-road crash scenarios are not considered.

We consider the most frequent on-road motorcycle crash scenarios in an urban area proposed by Piantini et al. [30], ISO 13232-2 [32] and MAIDS [28]. Here, only the frontal collision against a car and the collision of a car with the motorcycle's side are considered. In the future, additional crash scenarios, such as the collision of a car to the motorcycle's rear or single-vehicle accidents, should be accounted for.

We introduce the mechanical loads over the steering head, whereby not all load scenarios occurring in accidents can be reproduced. Experiments with an alternative load introduction should be conducted to consider additional load scenarios, e.g. flat loads that can occur when a car hits the motorcycle from the side.

Table 5. Results of CORA rating.

Load configuration	Rating method	Rating	Total rating
*V*1	Corridor method	0.737	0.781
	Correlation method	0.824	
*V*2	Corridor method	0.951	0.959
	Correlation method	0.968	
*V*3	Corridor method	0.888	0.930
	Correlation method	0.972	
*V*4	Corridor method	0.580	0.751
	Correlation method	0.922	
Total rating			0.855

The exact load conditions for the investigated motorcycle frame in normal operations are unknown. Therefore, we derived load configurations based on load scenarios proposed in the open literature for fatigue tests, stiffness characterisation or a design process of a motorcycle. We used the presented magnitudes of the normal operation forces only for the pre-loading to eliminate the clearances. Afterwards, we load the frame up to the maximum applicable load, respectively displacement of the test rig.

The study performs the experiments under quasi-static test load conditions. In future, the motorcycle frame should also be investigated under dynamic conditions to evaluate the dynamic effects of strain rates on mechanical behaviour.

4. Discussion

The presented dedicated test rig allows the investigation of a motorcycle frame's elastoplastic deformation and failure behaviour under four mechanical load configurations. The four load configurations represent load scenarios acting on a motorcycle frame in everyday usage (e.g. acceleration, cornering or braking, passing kerbs) and the most frequent crash scenarios (e.g. frontal collision) for an on-road motorcycle in urban areas. To investigate the elastoplastic deformation behaviour of the frame, the magnitude of the applied loads is multiple times higher than the maximum loads that occur in normal operation. The chosen force thresholds in pre-loading are appropriate because the offset does not affect the overall mechanical behaviour and occurs in the very first part of loading, where a linear mechanical behaviour dominates. The defined CORA parameters are suitable for the described application in this study, as the curves for each load configuration show good or excellent compliance that can also be visually observed. Nevertheless, despite the good reproducibility, some differences within the load configurations are obtained.

In *V*1, the bearings in the test with Frame 2 break consecutively one after the other and not simultaneously as in the other two tests. Additionally, it should be mentioned that the expected loads in normal operation are exceeded by approximately 50 kN. In *V*2, it can be stated that the expected maximum force in normal operation is outrun by two times. The deformation behaviour and the force–displacement curves behave similarly for all tests and do not show any anomalies. In *V*3, Frame 9 shows a drop in force that is not observed in the other tests. This results from a crack in the frame, which was observed 40–60% smaller form in the other two frames. Except for this drop in force, the overall behaviour and progression are comparable within the three tests. In *V*4, Frame 10 shows a different torque–rotation angle curve than the other two frames after around 8 kNm. Noticeably, at this torque, the slope changes from a linear incline to a more flattened slope. The further progression of the curves is similar, with the curve of Frame 10 shifted rearwards by 6°. These differences result from the plastic behaviour of the joints between the tubes, combined with different crack propagation at the welds.

In normal operation's expected maximum force range, all frames behave nearly identically within one load configuration. Furthermore, the progression of the load–displacement curves is very similar in the linear part without any exceptions. When the slope changes to a less steep incline, the behaviour of the frames start to differ slightly from each other due to fractions and plastic deformations. This can be explained by the complex frame structure consisting of different components, such as tubes with different cross sections and casting components joined by welding. Also, the propagation of fractures at the welding spots differs from frame to frame because of the manufacturing process (e.g. heat input during welding or tempering). Additionally, the manufacturing tolerances play a role in the collective behaviour since the frame consists of multiple individual components.

Based on the experiment results, the authors found that:

- In all experiments, the inner part of the frame remains nearly un-deformed. This un-deformed space could provide space for sensitive components (e.g. battery packs for EPTWs), which are essential to be protected from deformations.
- The deformation of the motorcycle frame in the load configurations $V1$ & $V4$ is comparable to the deformation occurring in full vehicle crash tests [37]. This shows that the simplifications for the crash scenario are applicable.
- In all load configurations, the linear part exceeds the expected maximum force of normal operation loads. Within the linear part, the load–displacement curves have a similar progression. After exceeding the linear part, the load–displacement curves start to differ for all load configurations because of the complex frame structure and the occurrence of plastification and fractures.
- The fractures do not occur directly at the welding points because of the assembling process. When a tube is welded to a casting part, a small part of the casting protrudes into the pipe. For this reason, and maybe of the different material structures in the heat-affected zone, failure does not occur directly at the welding point.
- The area of occurrence of fractures under elastoplastic deformation is similar to the one in fatigue tests [4,5]. These weak points are decisive for the crashworthiness and fatigue life.
- The applied approach of pre-loading shows a necessity to eliminate the clearance of the test rig and the frame due to manufacturing tolerances.

5. Conclusion

In conclusion, four different load configurations investigate the elastoplastic mechanical deformation behaviour of a motorcycle frame as an isolated component. These load configurations represent normal operating loads and the most frequent on-road crash scenario for a motorcycle in urban areas. A dedicated test rig with well-known boundary conditions is presented to measure the applied load and the resulting frame-only deformations of the frame in the four investigated load configurations. The pre- and post-measurements of the mechanical deformation of the frames show that the inner part of the frame remains nearly un-deformed. The CORA assessment supports the optical impression of a good reproducibility of the experiments.

The observed load–displacement curves and the deformation patterns of the investigated frames provide the basis for assessing the frame's crashworthiness and suitability as a protective structure for inner-placed components (e.g. a traction battery). Therefore, the following conclusions can be drawn:

- The motorcycle frame is suitable as a protective structure for sensitive components (e.g. battery packs) because the inner part of the frame remains nearly un-deformed in all load configurations. These findings correlate with full vehicle crash tests [10].
- The experiments show that fractures occur, similar to fatigue tests [4,5], in the area where different components are welded together. The information about these weak points of the frame can be used to improve the crashworthiness further.
- The observed deformation pattern and failure modes can be used to prove the mechanical elastoplastic behaviour of a simulation model.
- The deformation of the motorcycle frame as an isolated component is comparable to the deformation occurring in full vehicle crash tests in a frontal collision [37].
- The proposed parameters of the CORA method can be used to evaluate the quality of simulation models compared to experimental results in the future.
- The well-known boundary conditions, in combination with the presented measurement method, enable the use of the load–displacement curves to prove and validate a future motorcycle frame simulation model. Because the frame-only deformations are measured without the influence of the test rig, a simulation model can be validated without the need to model the entire test environment.

In this research, only quasi-static test configurations are investigated. Dynamic configurations will also be of interest for future analysis to establish whether frame behaviour in dynamic scenarios is comparable with the presented behaviour in quasi-static conditions. Furthermore, dynamic tests will provide information on the loads acting on the motorcycle frame in accident scenarios.

Author's contributions

Conceptualization, M.F. and C.E.; methodology, M.F., A.S. and C.E.; investigation, M.F., A.S. and C.E.; writing–original draft preparation, M.F.; writing–review and editing, M.F., A.S. and C.E.; visualisation, M.F and C.E.; supervision, C.E.; project administration, A.S. and C.E. All authors have read and agreed to the published version of the manuscript.

Acknowledgement

The authors extend their thanks to KTM AG for the provision of the frames and their cooperation during the project.

Disclosure statement

The authors declare that they have no known competing financial interests or personal relationships that could have appeared to influence the work reported in this article.

Funding

This work was conducted as part of the research project Future (project number: 854934), which was funded by the Austrian Research Promotion Agency (FFG). Open Access Funding by the Graz University of Technology.

ORCID

Markus Fasching http://orcid.org/0000-0002-3038-5955

References

[1] Cossalter V, Lot R, Massaro M. The influence of frame compliance and rider mobility on the scooter stability. Veh Syst Dyn. 2007;45(4):313–326.
[2] Cossalter V. Motorcycle dynamics. 2nd English ed.; Lulu: Padova, 2006, ISBN 1430308613.
[3] Sharp RS, Alstead CJ. The influence of structural flexibilities on the straight-running stability of motorcycles. Veh Syst Dyn. 1980;9(6):327–357.
[4] Petrone N, Meneghetti G. Fatigue life prediction of lightweight electric moped frames after field load spectra collection and constant amplitude fatigue bench tests. Int J Fatigue. 2019;127:564–575. doi: 10.1016/j.ijfatigue.2019.05.019.
[5] Petrone N, Saraceni M. Field load acquisition and variable amplitude fatigue testing on maxi-scooter motorcycles. Frattura Ed Integrità Strutturale. 2014;8(30):226–236. doi: 10.3221/IGF-ESIS.30.29.
[6] Tuluie R, Ericksen GS. Racing motorcycle design process using physical and virtual testing methods. Warrendale, PA; 2000; SAE Technical Paper 2000-01-3576, 2000, https://doi.org/10.4271/2000-01-3576.
[7] Peck L, Manning J, Bartlett W, et al. Eleven instrumented motorcycle crash tests and development of updated motorcycle impact-speed equations. *In* SAE Technical Paper Series. *WCX World Congress Experience, APR. 10, 2018; SAE International400 Commonwealth Drive, Warrendale, PA, United States, 2018,* https://doi.org/10.4271/2018-01-0517.
[8] Raffler M, Sinz W, Erker S, et al. Influence of loading rate and out of plane direction dependence on deformation and electro-mechanical failure behavior of a lithium-ion pouch cell. J Storage Mater. 2022;56:105906. doi: 10.1016/j.est.2022.105906.
[9] Ellersdorfer, C. Abbildung und bewertung des crashverhaltens von lithiumbasierten batterien für elektrisch betriebene motorräder. [Ph.D. Thesis, Technische Universität Graz, Graz, Austria, 2016].
[10] Ellersdorfer C, Sevarin A, Tomasch E, et al. Battery safety evaluation of electric driven motorcycles from the perspective of accident research. Electric vehicle Symposium; Stuttgart, 2017.
[11] Bisschop R, Willstrand O, Amon F, et al. Fire safety of lithium-ion batteries in road vehicles. Boras, Sweden: RISE Research Institute of Sweden; 2019.
[12] Lai X, Jin C, Yi W, et al. Mechanism, modeling, detection, and prevention of the internal short circuit in lithium-ion batteries: recent advances and perspectives. Energy Storage Mater. 2021;35:470–499. doi: 10.1016/j.ensm.2020.11.026.
[13] Kukreja J, Nguyen T, Siegmund T, et al. Crash analysis of a conceptual electric vehicle with a damage tolerant battery pack. Extreme Mech Lett. 2016;9:371–378. doi: 10.1016/j.eml.2016.05.004.
[14] Zhu J, Wierzbicki T, Li W. A review of safety-focused mechanical modeling of commercial lithium-ion batteries. J Power Sources. 2018;378:153–168. doi: 10.1016/j.jpowsour.2017.12.034.
[15] Macdonald MP, Chandrasekaran S, Garimella S, et al. Thermal runaway in a prismatic lithium ion cell triggered by a short circuit. J Storage Mater. 2021;40:102737. doi: 10.1016/j.est.2021.102737.
[16] Feng X, Ouyang M, Liu X, et al. Thermal runaway mechanism of lithium ion battery for electric vehicles: a review. Energy Storage Mater. 2018;10:246–267. doi: 10.1016/j.ensm.2017.05.013.
[17] Yang R, Xiong R, Ma S, et al. Characterization of external short circuit faults in electric vehicle li-ion battery packs and prediction using artificial neural networks. Appl Energy. 2020;260:114253. doi: 10.1016/j.apenergy.2019.114253.
[18] Sun J, Li J, Zhou T, et al. Toxicity, a serious concern of thermal runaway from commercial li-ion battery. Nano Energy. 2016;27:313–319. doi: 10.1016/j.nanoen.2016.06.031.
[19] Ballo F, Gobbi M, Massera M, et al., editors. A race motorcycle frame: advanced design. ASME; New York, USA, 2014. doi: 10.1115/DETC2014-34339.
[20] Sonsino C. Course of SN-curves especially in the high-cycle fatigue regime with regard to component design and safety. Int J Fatigue. 2007;29(12):2246–2258. doi: 10.1016/j.ijfatigue.2006.11.015.
[21] Cossalter V, Doria A, Lot R, et al. Dynamic properties of motorcycle and scooter tires: measurement and comparison. Veh Syst Dyn. 2003;39(5):329–352. doi: 10.1076/vesd.39.5.329.14145.
[22] de Vries EJH, Pacejka HB. Motorcycle tyre measurements AND models. Veh Syst Dyn. 1998;29(suppl1):280–298. doi: 10.1080/00423119808969565.
[23] Pacejka HB, editor. Tyre and vehicle dynamics. 2nd ed. Rotterdam: Elsevier; 2006.
[24] Bocciolone M, Cheli F, Pezzola M, et al., editors. Static and dynamic properties of a motorcycle frame: experimental and numerical approach. Twelfth International Conference on Computational Methods and Experimental Measurements - CMEM XII. Southampton: WIT Press; 2005.
[25] Cossalter V, Doria A, Massaro M, et al. Experimental and numerical investigation on the motorcycle front frame flexibility and its effect on stability. Mech Syst Sig Process. 2015;60–61:452–471. doi: 10.1016/j.ymssp.2015.02.011.
[26] Tan KS, Wong SV, Radin Umar RS, et al. An experimental study of deformation behaviour of motorcycle front wheel-tyre assembly under frontal impact loading. Int J Impact Eng. 2006;32(10):1554–1572. doi: 10.1016/j.ijimpeng.2005.04.007.
[27] Rane SS, Srividya A, Verma AK. Taguchi methods and finite element methods in reliability based crashworthiness and risk analysis of motorcycle frame. Int J Syst Assur Eng Manag. 2011;2(4):319–324. doi: 10.1007/s13198-012-0081-1.
[28] ACEM, Motorcycle Accident in Depth Study (MAIDS) - In-Depth investigations of accidents involving powered two wheelers; Brussels, 2009.
[29] Berg FA, Rücker P, König J. Motorcycle crash tests—an overview. Int J Crashworthines. 2005;10(4):327–339. doi: 10.1533/ijcr.2005.0349.
[30] Piantini S, Pierini M, Delogu M, et al. Injury analysis of powered two-wheeler versus other-vehicle urban accidents. In: 2016 IRCOBI Conference Proceedings. Malaga, Spain: IRCOBI; 2016.
[31] Grassi A, Baldanzini N, Barbani D, et al. A comparative analysis of MAIDS and ISO13232 databases for the identification of the most representative impact scenarios for powered 2-

wheelers in Europe. Traffic Inj Prev. 2018;19(7):766–772. doi: 10.1080/15389588.2018.1497791.

[32] International Organisation for Standardisation, ISO 13232-2:2005 Motorcycles - Test and analysis procedures for research evaluation of rider crash protective devices fitted to motorcycles; Switzerland, 2005.

[33] Santos K, Dias JP. Motorcycle accident reconstruction: influence of structural deformation or failure. Eng Fail Anal. 2020; 115:104597. doi: 10.1016/j.engfailanal.2020.104597.

[34] Klug C, Feist F, Raffler M, et al. Development of a procedure to compare kinematics of human body models for pedestrian simulations. In: 2017 IRCOBI Conference Proceedings. Antwerp, Belgium: IRCOBI; 2017. p. 509–530.

[35] Sevarin A, Fasching M, Ellersdorfer C. Crash safety optimisation method for the integration of the traction batteries into electric powered-two-wheelers. In: Tagungsband der 13. Internationalen Motorradkonferenz 2020, ifz Institut für Zweiradsicherheit e.V.

[36] Fasching M. Optimization of an EPTW battery pack as a structural component to improve the crashworthiness, In RedCabin: Next Generation 48 V in Automotive, RedCabin, online, webinar; 2021

[37] Ellersdorfer C, Sevarin A, Tomasch E, et al. Evaluation method of the crash safety of traction batteries for electric driven motorcycles. In Tagungsband der 11. Internationalen Motorradkonferenz; ifz Institut für Zweiradsicherheit e.V, Ed.; ifz Institut für Zweiradsicherheit e.V: Essen, 2016, ISBN 3923994222.

[38] Chawla A, Mukherjee S, Mohan D, et al. FE simulations of motorcycle—car frontal crashes, validations and observations. Int J Crashworthines. 2005;10(4):319–326. doi: 10.1533/ijcr.2005.0344.

[39] Isaac CW, Ezekwem C. A review of the crashworthiness performance of energy absorbing composite structure within the context of materials, manufacturing and maintenance for sustainability. Compos Struct. 2021;257:113081. doi: 10.1016/j.compstruct.2020.113081.

[40] Gehre C. CORAplus Release 4.0.4; pdb—Partnership for Dummy Technology and Biomechanics: Gaimersheim, Germany, 2017.

[41] Gehre C, Gades H, Wernicke P. Objective rating of signals using test and simulation responses. In: The 21st ESV Conference Proceedings. Stuttgart, Germany: NHTSA; 2009. p. 1–8.

[42] Barbat S, Fu Y, Zhan Z, et al. Objective rating metric for dynamic systems. In: The 23rd ESV Conference Proceedings. Seoul, Republic of Korea: NHTSA; 2013. p. 1–10.

[43] Giordano C, Kleiven S. Development of an unbiased validation protocol to assess the biofidelity of finite element head models used in prediction of traumatic brain injury. Stapp Car Crash J. 2016;60:363–471.

[44] Somasundaram K, Zhang L, Sherman D, et al. Evaluating thoracolumbar spine response during simulated underbody blast impact using a total human body finite element model. J Mech Behav Biomed Mater. 2019;100:103398. doi: 10.1016/j.jmbbm.2019.103398.

[45] Thunert C. CORAplus Release 4.0.4: User's Manual, *Braunschweig, Germany, 2017. Available online: https://www.pdb-org.com/en/information/18-cora-download.html (accessed on 10 December 2022).*

[46] Murmann R, Harzheim L, Dominico S, et al. CoSi: correlation of signals—a new measure to assess the correlation of history response curves. Mech Syst Sig Process. 2016;80:482–502. doi: 10.1016/j.ymssp.2016.04.026.

[47] ISO. Road vehicles - Objective rating metric for non-ambiguous signals ISO/TS 18571:2014(E), 2014 (cited 2020 Jan 29).